Supplement of Clim. Past, 21, 1633–1660, 2025
https://doi.org/10.5194/cp-21-1633-2025-supplement

Climate of the Past
Open Access
EGU

Supplement of

Perspective on ice age terminations from absolute chronologies provided by global speleothem records

Nikita Kaushal et al.

Correspondence to: Nikita Kaushal (nikitageologist@gmail.com)

Supplementary Information

Table S1: Further information of speleothem entities that were not analysed as a part of the main manuscript since they only partially cover Terminations or have lower resolution or U-Th dates with larger errors than the records used in the main manuscript. Cave site locations are plotted in Fig. S1 and time series plots are in Fig. S2. Some data from the main manuscript are included in the table and plots to enable comparison.

region	site name	latitude	longitude	elev. (m)	entity name	age model	citation	primary interpretation	secondary interpretation	comments
South Europe	Corchia	43.9833	10.2167	840	CC-5_2018	SISAL-Bchron	Tzedakis et al., 2018	rainfall amount	source water composition	
					CC-1_2018	SISAL-copRa	Tzedakis et al., 2017	rainfall amount	source water composition	
	Soreq	31.7558	35.0226	400	Soreq_composite (green)	author-linear between dates	Bar-Matthews et al., 2003	rainfall amount	source water composition	composite includes stalactites;
	Jerusalem West	31.7833	35.15	700	AF12 (blue)	author-polynomial fit	Frumkin et al., 1999	source water composition	change in moisture transport trajectory and linked seasonality	age reversals beyond 100k; calcite precipitation T and ice volume source composition
	La Vallina	43.4100	-4.8067	70	Garth	author-mixed Bchron	Stoll et al., 2022	source water composition	temperature dependency of meteoric precipitation	confocal band counting
	Villars	45.43	0.78	175	Vil-car1	author-linear between dates	Wainer et al., 2011	cave air temperature	disequilibrium	flowstone; authors flag possible detrital contamination and U-leaching giving older ages,
North Europe	Abaliget	46.1333	18.1167	209	ABA_1	author-StalAge	Koltai et al., 2017	temperature dependency of meteoric precipitation	source water composition	flowstone; author generated age model uses both cores to create master chronology
	Schneckenloch	47.4333	9.8667	1285	SCH-5	SISAL-copRa	Moseley et al., 2015	temperature dependency of meteoric precipitation	change in moisture transport trajectory	
	Sieben Hengste	46.75	7.81	1955	7H-12	author-StalAge	Luetscher et al., 2021	temperature dependency of meteoric precipitation	change in moisture transport trajectory	
	Neotektonik	46.7833	8.2666	1700	M37-1-16A	author-OxCal	Wilcox et al., 2020			paper focused on fluid inclusions, no $\delta^{18}O$ interpretations provided; no reported hiatus
North America	Lehman caves	39.01	-114.22	2080	LMC-14	SISAL-copRa	Lachniet et al., 2014	temperature dependency of meteoric precipitation	change in moisture source latitude	
					LMC-21	SISAL-copRa	Lachniet et al., 2014	temperature dependency of meteoric precipitation	change in moisture source latitude	
					LC-2	SISAL-Bchron	Shakun et al., 2011			
	Devils Hole	36.4254	-116.2915	719	DH2-D	author-OxCal	Moseley et al., 2016	temperature dependency of meteoric precipitation	change in seasonality	sub-aqueous calcite; shallowest core with least 230Th effect and youngest chronologies

EASM	Dongge	25.2833	108.0833	680	D4_2005_Kelly	author-unknown	Kelly et al., 2006	change in seasonality	upstream rainout	
					D8	SISAL-copRa	Kelly et al., 2006	change in seasonality	upstream rainout	
	Sanbao	31.667	110.4333	1900	SB11	sisal-copRa	Cheng et al., 2016b	upstream rainout	change in seasonality	
					SB23	sisal-copRa	Cheng et al., 2016b	upstream rainout	change in seasonality	
					SB25-2	sisal-copRa	Cheng et al., 2016b	upstream rainout	change in seasonality	
					SB41	sisal-copRa	Cheng et al., 2016b	upstream rainout	change in seasonality	
South Europe	Sofular	41.4167	31.9333	440	SO-4	SISAL-Bchron	Badertscher et al., 2011	source water composition		more negative from Caspian Sea with melt waters, more positive from Mediterranean
	Crovassa Azzurra	39.28	8.48	410	CA	author-linear between dates	Columbu et al., 2019	rainfall amount	change in moisture source	flowstone; mixed mineralogy-aragonite with some calcite
	Peqiin cave	32.58	35.19	650	PEK_composite	author-unknown	Bar-Matthews et al., 2003	rainfall amount	source water composition	composite includes stalactites
	Ejulve	40.76	-0.59	1240	ARTEMISA	author-StalAge and other	Pérez-Mejías et al., 2017	temperature change	source water composition	record focuses on $\delta^{13}C$ as proxy for dry conditions
Central Asia	Kesang	42.87	81.75	2000	KS06-A	SISAL-copRa	Cheng et al., 2016a	large-scale circulation and supra-regional climate	change in moisture transport trajectory and linked seasonality	temperature effect on calcite precipitation
	Kesang	42.87	81.75	2000	KS08-1	SISAL-copRa	Cheng et al., 2016a	large-scale circulation and supra-regional climate	change in moisture transport trajectory and linked seasonality	temperature effect on calcite precipitation
ISM	Xiaobailong	24.2	103.36	1500	XBL-26	SISAL-copRa	Cai et al., 2015	rainfall amount		
	Bittoo	30.7903	77.7764	3000	BT-9	sisal-Bchron	Kathayat et al., 2016	large-scale circulation, upstream changes, moisture transport history		

Figure S1: Plots of speleothem entities that were not analysed as a part of the main manuscript since they only partially cover Terminations or have lower resolution or U-Th dates with larger errors than the records used in the main manuscript or are composite records. Key plots from the main manuscript have also been shown in these supplementary figures for comparison. Ages covering Terminations in kilo years before 1950 (ky BP) are plotted against oxygen isotopic measurements in ‰. The direction of the Y axis for each figure has been selected so that up points to warmer or wetter climates. Age-depth model uncertainties where available are plotted as grey shading on the proxy plots. U-Th dates and dating uncertainties have been plotted below the proxy plots. Insolation curves in Wm^{-2} are plotted in sub-figures '(a)' of each of the Termination figures and are the summer half year caloric insolation as provided in Tzedakis et al, 2017. This metric for insolation was selected because it accounts for the effect of both precession and obliquity on northern latitude insolation. Cave sites are shown on maps in Fig.1 and further record information can be found in Table S1. Since a large number of records are available for Termination II, separate plot sections have been made for North Europe, North America and the monsoon records respectively.

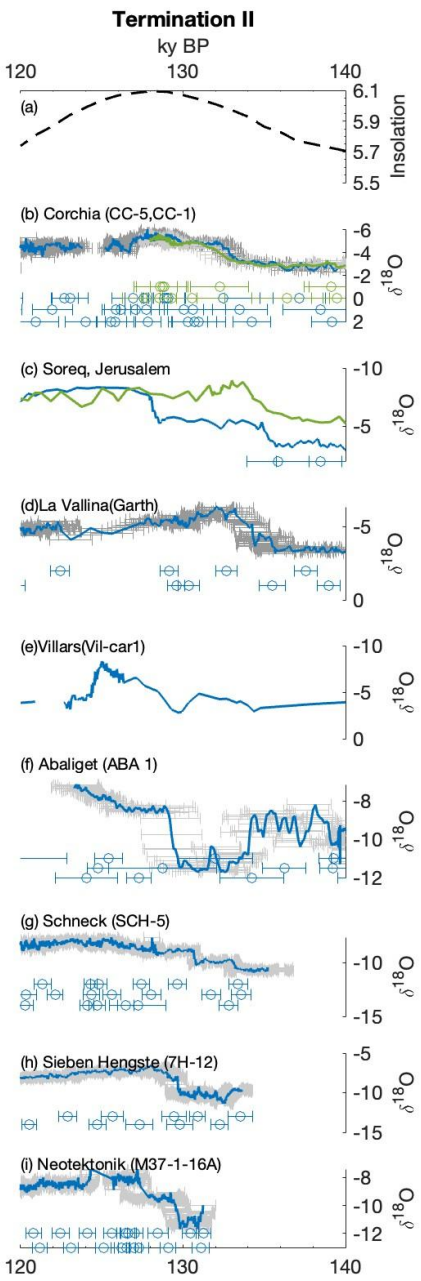
Termination II
ky BP
120
130
140
(a)
6.1
5.9
5.7
5.5
Insolation
(b) Corchia (CC-5,CC-1)
-6
-4
-2
0
2
δ18O
(c) Soreq, Jerusalem
-10
-5
(d)La Vallina(Garth)
-5
0
(e)Villars(Vil-car1)
-10
-5
0
(f) Abaliget (ABA 1)
-8
-10
-12
(g) Schneck (SCH-5)
-10
-15
(h) Sieben Hengste (7H-12)
-5
-10
-15
(i) Neotektonik (M37-1-16A)
-8
-10
-12
120
130
140

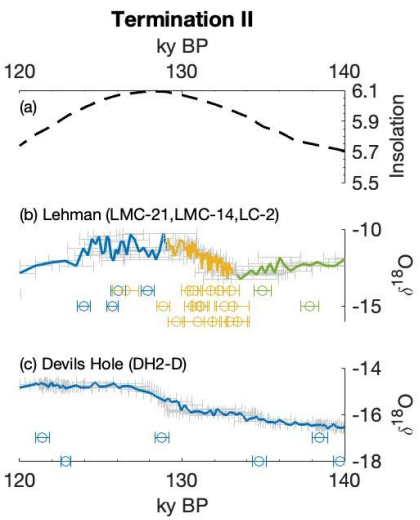
Termination II
ky BP
120
130
140
(a)
6.1
5.9
5.7
5.5
Insolation
(b) Lehman (LMC-21,LMC-14,LC-2)
-10
-15
δ18O
(c) Devils Hole (DH2-D)
-14
-16
-18
120
130
140
ky BP

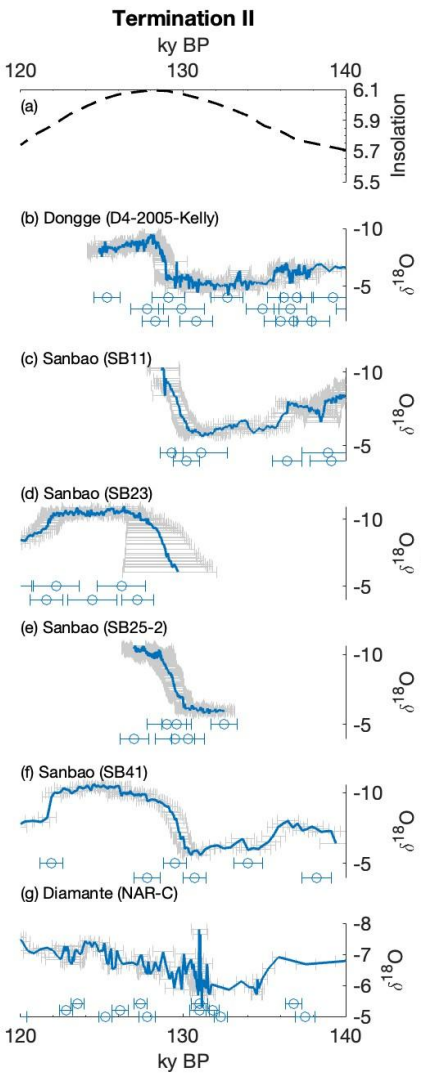
Termination II
ky BP
120
130
140
(a)
6.1
5.9
5.7
5.5
Insolation
(b) Dongge (D4-2005-Kelly)
-10
-5
δ18O
(c) Sanbao (SB11)
-10
-5
(d) Sanbao (SB23)
-10
-5
(e) Sanbao (SB25-2)
-10
-5
(f) Sanbao (SB41)
-10
-5
(g) Diamante (NAR-C)
-8
-7
-6
-5
120
130
140
ky BP

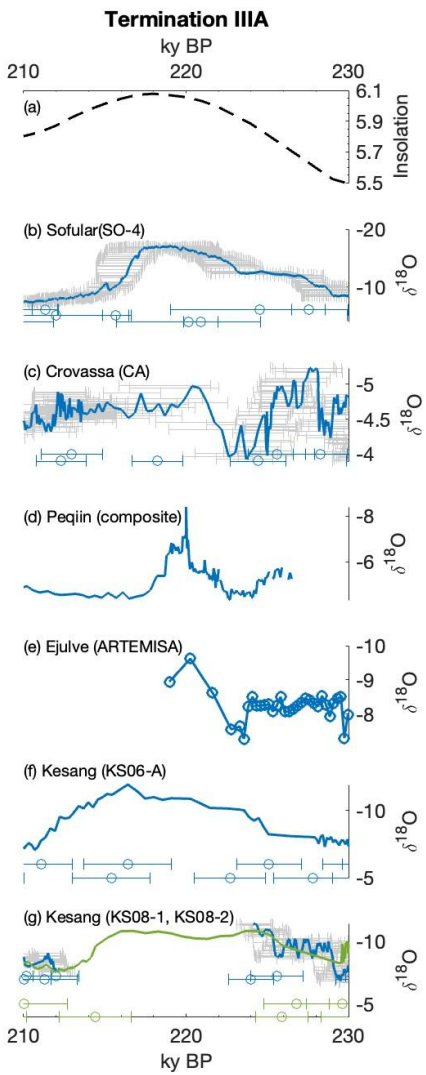
Termination IIIA
ky BP
210
220
230
(a)
6.1
5.9
5.7
5.5
Insolation
(b) Sofular(SO-4)
-20
-10
δ18O
(c) Crovassa (CA)
-5
-4.5
-4
(d) Peqiin (composite)
-8
-6
(e) Ejulve (ARTEMISA)
-10
-9
-8
(f) Kesang (KS06-A)
-10
-5
(g) Kesang (KS08-1, KS08-2)
-10
-5
210
220
230
ky BP

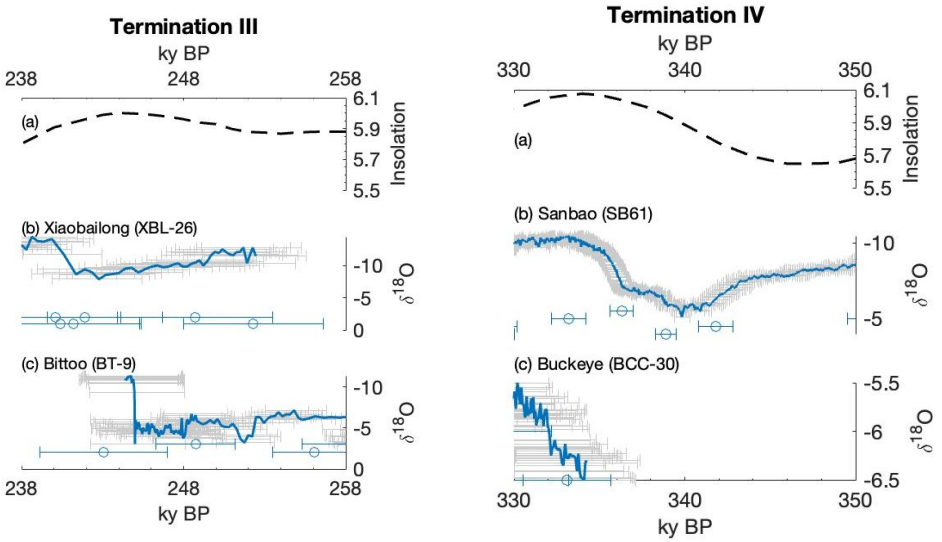
Termination III
ky BP
238
248
258
(a)
6.1
5.9
5.7
5.5
Insolation
(b) Xiaobailong (XBL-26)
-10
-5
0
δ18O
(c) Bittoo (BT-9)
-10
-5
0
δ18O
238
248
258
ky BP
Termination IV
ky BP
330
340
350
(a)
6.1
5.9
5.7
5.5
Insolation
(b) Sanbao (SB61)
-10
-5
δ18O
(c) Buckeye (BCC-30)
-5.5
-6
-6.5
δ18O
330
340
350
ky BP

Figure S2: Ages covering Terminations are plotted against **(a)** insolation, **(b)** sea level curves and **(c)** the ice volume effects on seawater oxygen isotopic records. Insolation curves in Wm^{-2} are plotted in sub-figures '(a)' of each of the Termination figures and are the summer half year caloric insolation as provided in Tzedakis et al, 2017. This metric for insolation was selected because it accounts for the effect of both precession and obliquity on northern latitude insolation. The Spratt and Lisiecki sea level curve is based on orbital tuning, and the Grant sea level curve is based on tuning to millennial dust events in the Red Sea. These two curves exhibit difference in timing and amplitude of sea level rise during Terminations and this is shown in the figures. The benthic derived Waelbroeck sea level curve has a lower resolution and has not been used for further calculations but has also been plotted here. A value of 0.00833 ‰ / m of relative sea level has been used to calculate the global average change in $\delta^{18}O_{seawater.}$ For Termination II, the North Iberian Speleothem Archive (NISA) record is superimposed over the global curves to showcase the impact of regional North Atlantic changes in sea water $\delta^{18}O$ compared to the global curves.

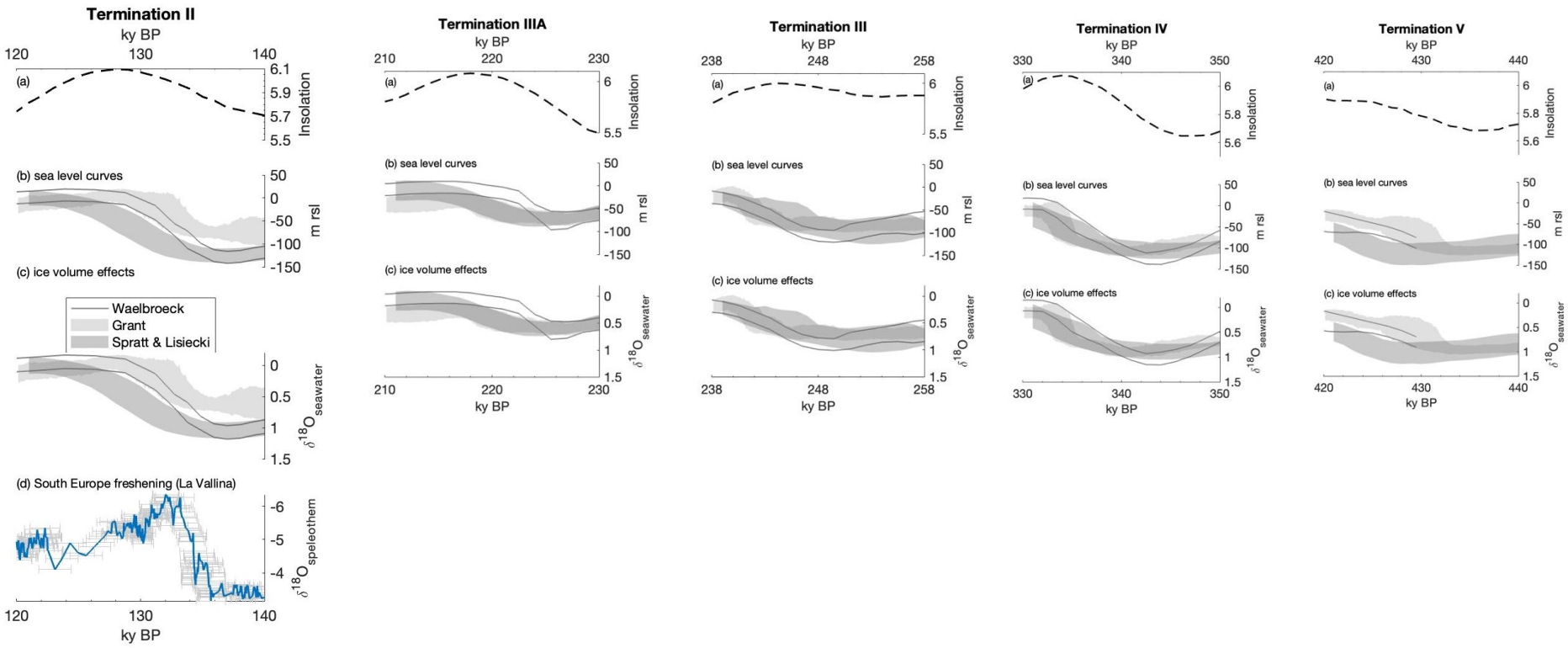
Termination II
ky BP
120
130
140
(a)
6.1
5.9
5.7
5.5
Insolation
(b) sea level curves
50
0
-50
-100
-150
m rsl
(c) ice volume effects
Waelbroeck
Grant
Spratt & Lisiecki
0
0.5
1
1.5
δ18Oseawater
(d) South Europe freshening (La Vallina)
-6
-5
-4
δ18Ospeleothem
120
130
140
ky BP
Termination IIIA
ky BP
210
220
230
(a)
6
5.5
Insolation
(b) sea level curves
50
0
-50
-100
-150
m rsl
(c) ice volume effects
0
0.5
1
1.5
δ18Oseawater
210
220
230
ky BP
Termination III
ky BP
238
248
258
(a)
6
5.5
Insolation
(b) sea level curves
50
0
-50
-100
-150
m rsl
(c) ice volume effects
0
0.5
1
1.5
δ18Oseawater
238
248
258
ky BP
Termination IV
ky BP
330
340
350
(a)
6
5.8
5.6
Insolation
(b) sea level curves
50
0
-50
-100
-150
m rsl
(c) ice volume effects
0
0.5
1
1.5
δ18Oseawater
330
340
350
ky BP
Termination V
ky BP
420
430
440
(a)
6
5.8
5.6
Insolation
(b) sea level curves
50
0
-50
-100
-150
m rsl
(c) ice volume effects
0
0.5
1
1.5
δ18Oseawater
420
430
440
ky BP

Figure S3: Ages covering Terminations are plotted against the ice volume effects on speleothem oxygen isotopic records. Insolation curves in Wm^{-2} are plotted in the first sub-figures at the top of each Termination plot and are the summer half year caloric insolation as provided in Tzedakis et al, 2017. This metric for insolation was selected because it accounts for the effect of both precession and obliquity on northern latitude insolation. The Spratt and Lisiecki sea level curve is based on orbital tuning, and the Grant sea level curve is based on tuning to millennial dust events in the Red Sea. These two curves exhibit difference in timing and amplitude of sea level rise during Terminations and this is shown in the figures. For Termination II, the North Iberian Speleothem Archive (NISA) record is superimposed over the Europe speleothem data to showcase the impact of regional North Atlantic changes in sea water $\delta^{18}O$ compared to the global curves.

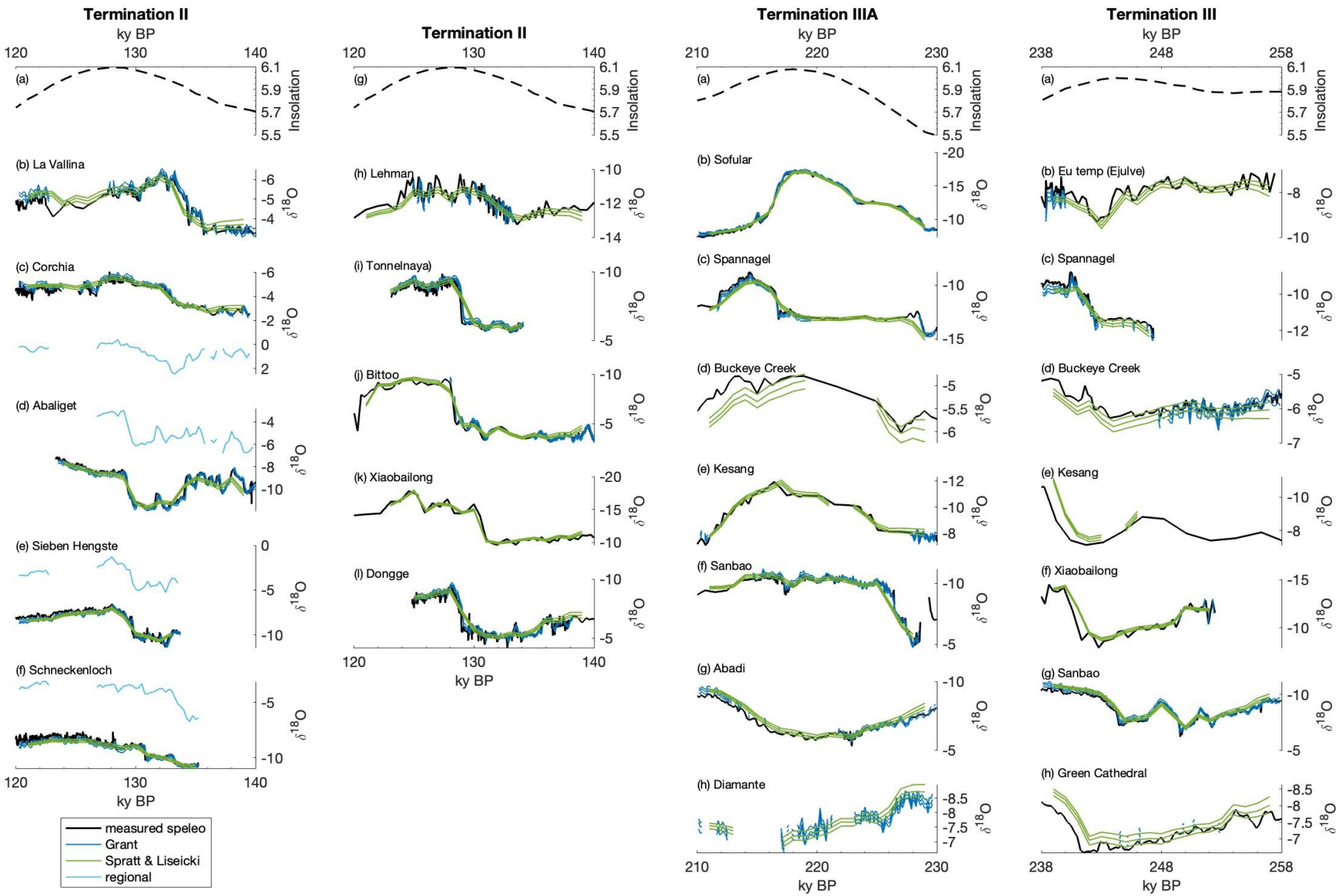
Termination II
ky BP
120
130
140
(a)
6.1
5.9
5.7
5.5
Insolation
(b) La Vallina
-6
-5
-4
δ18O
(c) Corchia
-6
-4
-2
0
2
δ18O
(d) Abaliget
-4
-6
-8
-10
δ18O
(e) Sieben Hengste
0
-5
-10
δ18O
(f) Schneckenloch
-5
-10
δ18O
120
130
140
ky BP
measured speleo
Grant
Spratt & Liseicki
regional
Termination II
ky BP
120
130
140
(g)
6.1
5.9
5.7
5.5
Insolation
(h) Lehman
-10
-12
-14
δ18O
(i) Tonnelnaya)
-10
-5
δ18O
(j) Bittoo
-10
-5
δ18O
(k) Xiaobailong
-20
-15
-10
δ18O
(l) Dongge
-10
-5
δ18O
120
130
140
ky BP
Termination IIIA
ky BP
210
220
230
(a)
6.1
5.9
5.7
5.5
Insolation
(b) Sofular
-20
-15
-10
δ18O
(c) Spannagel
-10
-15
δ18O
(d) Buckeye Creek
-5
-5.5
-6
δ18O
(e) Kesang
-12
-10
-8
δ18O
(f) Sanbao
-10
-5
δ18O
(g) Abadi
-10
-5
δ18O
(h) Diamante
-8.5
-8
-7.5
-7
δ18O
210
220
230
ky BP
Termination III
ky BP
238
248
258
(a)
6.1
5.9
5.7
5.5
Insolation
(b) Eu temp (Ejulve)
-8
-10
δ18O
(c) Spannagel
-10
-12
δ18O
(d) Buckeye Creek
-5
-6
-7
δ18O
(e) Kesang
-10
-8
δ18O
(f) Xiaobailong
-15
-10
δ18O
(g) Sanbao
-10
-5
δ18O
(h) Green Cathedral
-8.5
-8
-7.5
-7
δ18O
238
248
258
ky BP

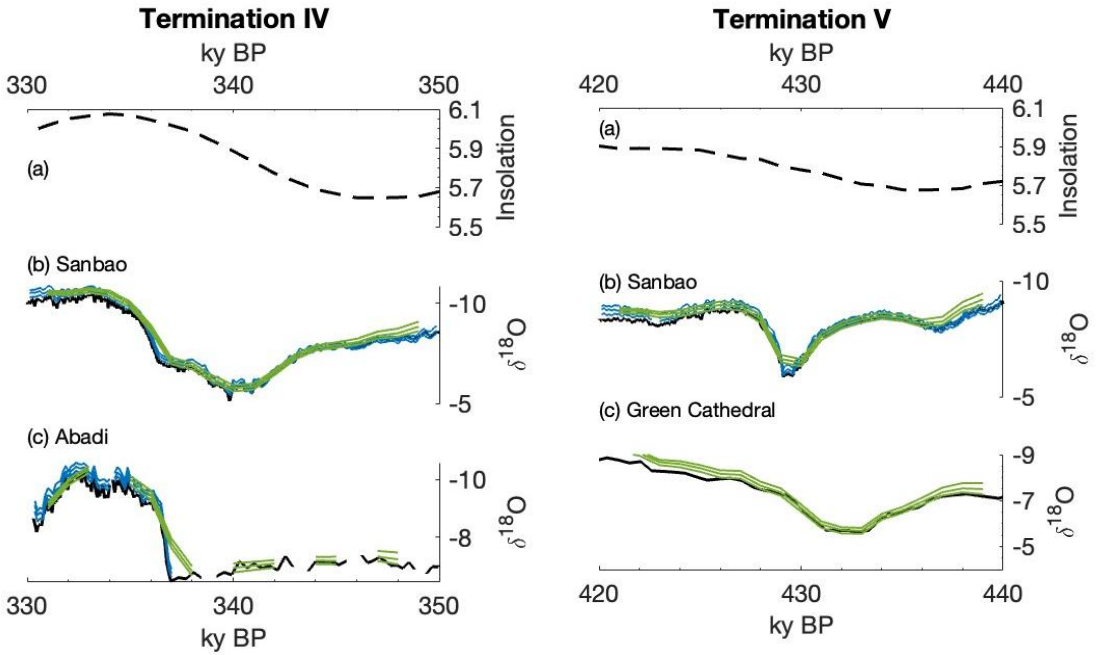
Termination IV
ky BP
330
340
350
(a)
6.1
5.9
5.7
5.5
Insolation
(b) Sanbao
-10
-5
$\delta^{18}O$
(c) Abadi
-10
-8
$\delta^{18}O$
330
340
350
ky BP
Termination V
ky BP
420
430
440
(a)
6.1
5.9
5.7
5.5
Insolation
(b) Sanbao
-10
-5
$\delta^{18}O$
(c) Green Cathedral
-9
-7
-5
$\delta^{18}O$
420
430
440
ky BP

Figure S4: Ages covering Terminations for the South European records from La Vallina and Ejulve caves are plotted against measured $\delta^{13}C$, degassing corrected $\delta^{13}C$ ($\delta^{13}C_{corr}$) and Mg/Ca records. The $\delta^{13}C_{corr}$ values are derived from an index based on the Mg/Ca data providing $\delta^{13}C$ 'initial' values that give temperature information.

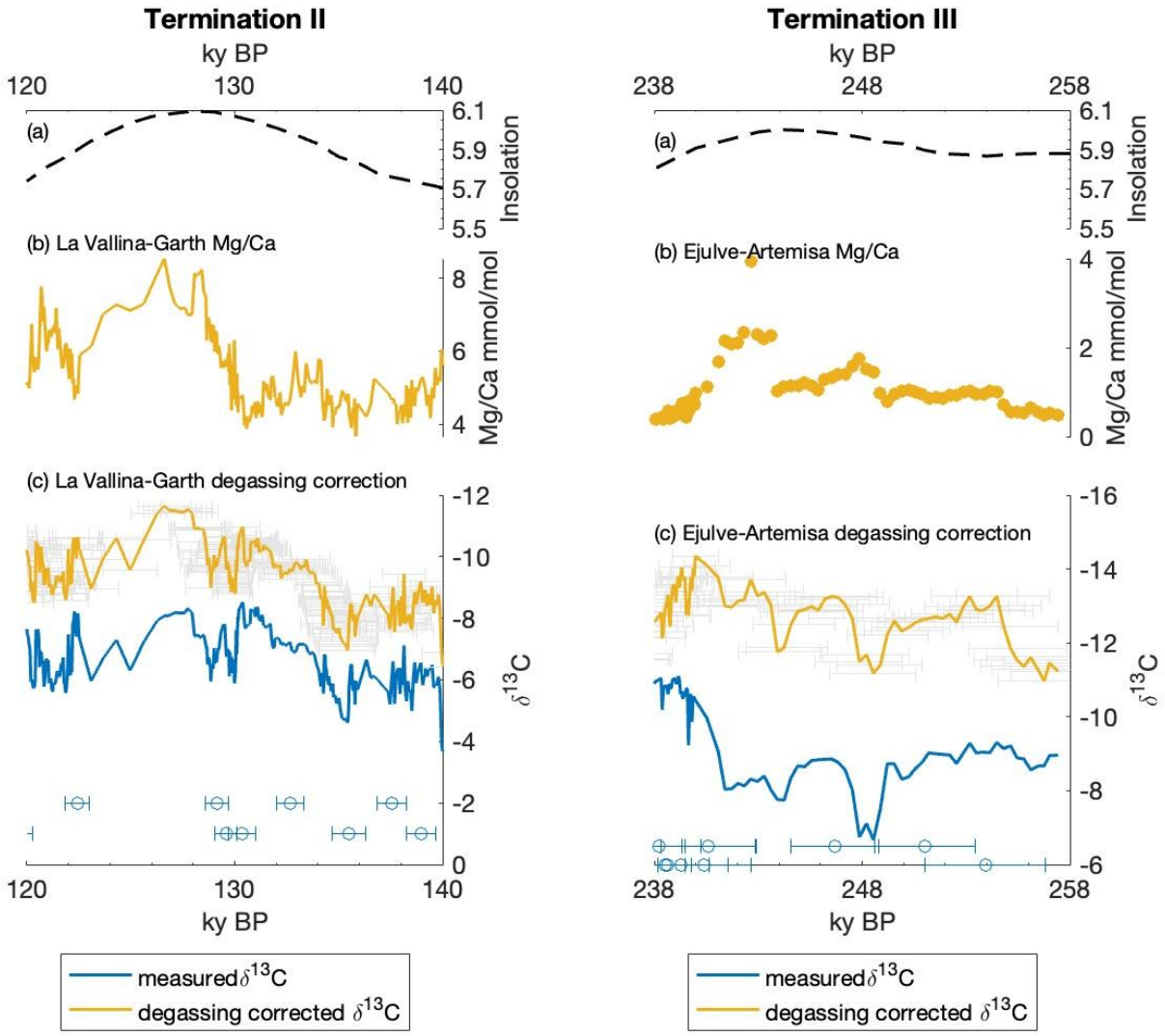
Termination II
ky BP
120
130
140
(a)
6.1
5.9
5.7
5.5
Insolation
(b) La Vallina-Garth Mg/Ca
8
6
4
Mg/Ca mmol/mol
(c) La Vallina-Garth degassing correction
-12
-10
-8
-6
-4
-2
0
δ^{13}C
120
130
140
ky BP
measured δ^{13}C
degassing corrected δ^{13}C
Termination III
ky BP
238
248
258
(a)
6.1
5.9
5.7
5.5
Insolation
(b) Ejulve-Artemisa Mg/Ca
4
2
0
Mg/Ca mmol/mol
(c) Ejulve-Artemisa degassing correction
-16
-14
-12
-10
-8
-6
δ^{13}C
238
248
258
ky BP
measured δ^{13}C
degassing corrected δ^{13}C

Badertscher, S., Fleitmann, D., Cheng, H., Edwards, R. L., Göktürk, O. M., Zumbühl, A., Leuenberger, M., and Tüysüz, O.: Pleistocene water intrusions from the Mediterranean and Caspian seas into the Black Sea, Nat. Geosci., 4, 236–239, https://doi.org/10.1038/ngeo1106, 2011.

Bar-Matthews, M., Ayalon, A., Gilmour, M., Matthews, A., and Hawkesworth, C. J.: Sea–land oxygen isotopic relationships from planktonic foraminifera and speleothems in the Eastern Mediterranean region and their implication for paleorainfall during interglacial intervals, Geochim. Cosmochim. Acta, 67, 3181–3199, https://doi.org/10.1016/S0016-7037(02)01031-1, 2003.

Cai, Y., Fung, I. Y., Edwards, R. L., An, Z., Cheng, H., Lee, J.-E., Tan, L., Shen, C.-C., Wang, X., Day, J. A., Zhou, W., Kelly, M. J., and Chiang, J. C. H.: Variability of stalagmite-inferred Indian monsoon precipitation over the past 252,000 y, Proc. Natl. Acad. Sci., 112, 2954–2959, https://doi.org/10.1073/pnas.1424035112, 2015.

Cheng, H., Spötl, C., Breitenbach, S. F. M., Sinha, A., Wassenburg, J. A., Jochum, K. P., Scholz, D., Li, X., Yi, L., Peng, Y., Lv, Y., Zhang, P., Votintseva, A., Loginov, V., Ning, Y., Kathayat, G., and Edwards, R. L.: Climate variations of Central Asia on orbital to millennial timescales, Sci. Rep., 6, 36975, https://doi.org/10.1038/srep36975, 2016a.

Cheng, H., Edwards, R. L., Sinha, A., Spötl, C., Yi, L., Chen, S., Kelly, M., Kathayat, G., Wang, X., Li, X., Kong, X., Wang, Y., Ning, Y., and Zhang, H.: The Asian monsoon over the past 640,000 years and ice age terminations, Nature, 534, 640–646, https://doi.org/10.1038/nature18591, 2016b.

Columbu, A., Spötl, C., De Waele, J., Yu, T.-L., Shen, C.-C., and Gázquez, F.: A long record of MIS 7 and MIS 5 climate and environment from a western Mediterranean speleothem (SW Sardinia, Italy), Quat. Sci. Rev., 220, 230–243, https://doi.org/10.1016/j.quascirev.2019.07.023, 2019.

Frumkin, A., Ford, D. C., and Schwarcz, H. P.: Continental Oxygen Isotopic Record of the Last 170,000 Years in Jerusalem, Quat. Res., 51, 317–327, https://doi.org/10.1006/qres.1998.2031, 1999.

Kathayat, G., Cheng, H., Sinha, A., Spötl, C., Edwards, R. L., Zhang, H., Li, X., Yi, L., Ning, Y., Cai, Y., Lui, W. L., and Breitenbach, S. F. M.: Indian monsoon variability on millennial-orbital timescales, Sci. Rep., 6, 24374, https://doi.org/10.1038/srep24374, 2016.

Kelly, M. J., Edwards, R. L., Cheng, H., Yuan, D., Cai, Y., Zhang, M., Lin, Y., and An, Z.: High resolution characterization of the Asian Monsoon between 146,000 and 99,000 years B.P. from Dongge Cave, China and global correlation of events surrounding Termination II, Palaeogeogr. Palaeoclimatol. Palaeoecol., 236, 20–38, https://doi.org/10.1016/j.palaeo.2005.11.042, 2006.

Koltai, G., Spötl, C., Shen, C.-C., Wu, C.-C., Rao, Z., Palcsu, L., Kele, S., Surányi, G., and Bárány-Kevei, I.: A penultimate glacial climate record from southern Hungary, J. Quat. Sci., 32, 946–956, https://doi.org/10.1002/jqs.2968, 2017.

Lachniet, M. S., Denniston, R. F., Asmerom, Y., and Polyak, V. J.: Orbital control of western North America atmospheric circulation and climate over two glacial cycles, Nat. Commun., 5, 3805, https://doi.org/10.1038/ncomms4805, 2014.

Luetscher, M., Moseley, G. E., Festi, D., Hof, F., Edwards, R. L., and Spötl, C.: A Last Interglacial speleothem record from the Sieben Hengste cave system (Switzerland): Implications for alpine paleovegetation, Quat. Sci. Rev., 262, 106974, https://doi.org/10.1016/j.quascirev.2021.106974, 2021.

Moseley, G. E., Spötl, C., Cheng, H., Boch, R., Min, A., and Edwards, R. L.: Termination-II interstadial/stadial climate change recorded in two stalagmites from the north European Alps, Quat. Sci. Rev., 127, 229–239, https://doi.org/10.1016/j.quascirev.2015.07.012, 2015.

Moseley, G. E., Edwards, R. L., Wendt, K. A., Cheng, H., Dublyansky, Y., Lu, Y., Boch, R., and Spötl, C.: Reconciliation of the Devils Hole climate record with orbital forcing, Science, 351, 165–168, https://doi.org/10.1126/science.aad4132, 2016.

Pérez-Mejías, C., Moreno, A., Sancho, C., Bartolomé, M., Stoll, H., Cacho, I., Cheng, H., and Edwards, R. L.: Abrupt climate changes during Termination III in Southern Europe, Proc. Natl. Acad. Sci., 114, 10047–10052, https://doi.org/10.1073/pnas.1619615114, 2017.

Shakun, J. D., Burns, S. J., Clark, P. U., Cheng, H., and Edwards, R. L.: Milankovitch-paced Termination II in a Nevada speleothem?, Geophys. Res. Lett., 38, https://doi.org/10.1029/2011GL048560, 2011.

Stoll, H. M., Cacho, I., Gasson, E., Sliwinski, J., Kost, O., Moreno, A., Iglesias, M., Torner, J., Perez-Mejias, C., Haghipour, N., Cheng, H., and Edwards, R. L.: Rapid northern hemisphere ice sheet melting during the penultimate deglaciation, Nat. Commun., 13, 3819, https://doi.org/10.1038/s41467-022-31619-3, 2022.

Tzedakis, P. C., Crucifix, M., Mitsui, T., and Wolff, E. W.: A simple rule to determine which insolation cycles lead to interglacials, Nature, 542, 427–432, https://doi.org/10.1038/nature21364, 2017.

Tzedakis, P. C., Drysdale, R. N., Margari, V., Skinner, L. C., Menviel, L., Rhodes, R. H., Taschetto, A. S., Hodell, D. A., Crowhurst, S. J., Hellstrom, J. C., Fallick, A. E., Grimalt, J. O., McManus, J. F., Martrat, B., Mokeddem, Z., Parrenin, F., Regattieri, E., Roe, K., and Zanchetta, G.: Enhanced climate instability in the North Atlantic and southern Europe during the Last Interglacial, Nat. Commun., 9, 4235, https://doi.org/10.1038/s41467-018-06683-3, 2018.

Wainer, K., Genty, D., Blamart, D., Daëron, M., Bar-Matthews, M., Vonhof, H., Dublyansky, Y., Pons-Branchu, E., Thomas, L., van Calsteren, P., Quinif, Y., and Caillon, N.: Speleothem record of the last 180 ka in Villars cave (SW France): Investigation of a large δ18O shift between MIS6 and MIS5, Quat. Sci. Rev., 30, 130–146, https://doi.org/10.1016/j.quascirev.2010.07.004, 2011.

Wilcox, P. S., Honiat, C., Trüssel, M., Edwards, R. L., and Spötl, C.: Exceptional warmth and climate instability occurred in the European Alps during the Last Interglacial period, Commun. Earth Environ., 1, 1–6, https://doi.org/10.1038/s43247-020-00063-w, 2020.